Journal of Colloid and Interface Science 448 (2015) 1–7

Contents lists available at ScienceDirect

Journal of Colloid and Interface Science

www.elsevier.com/locate/jcis

Strontium and zoledronate hydroxyapatites graded composite coatings for bone prostheses

Elisa Boanini [a,*], Paola Torricelli [b,c], Felix Sima [d], Emanuel Axente [d], Milena Fini [b,c], Ion N. Mihailescu [d], Adriana Bigi [a]

[a] Department of Chemistry "G. Ciamician", University of Bologna, 40126 Bologna, Italy
[b] Laboratory of Preclinical and Surgical Studies, Codivilla-Putti Research Institute, Rizzoli Orthopaedic Institute, Bologna, Italy
[c] Department Rizzoli RIT, Rizzoli Orthopedic Institute-IOR, Laboratory of Biocompatibility, Technological Innovations and Advanced Therapies, Bologna, Italy
[d] National Institute for Lasers, Plasma and Radiation Physics, P. O. Box MG 36, 77125 Bucharest-Magurele, Romania

GRAPHICAL ABSTRACT

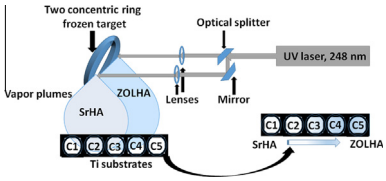

ARTICLE INFO

Article history:
Received 5 November 2014
Accepted 31 January 2015
Available online 9 February 2015

Keywords:
Combinatorial-MAPLE
Coatings
Strontium
Zoledronate
Hydroxyapatite
Co-cultures

ABSTRACT

Both strontium and zoledronate (ZOL) are known to be useful for the treatment of bone diseases associated to the loss of bone substance. In this work, we applied an innovative technique, Combinatorial Matrix-Assisted Pulsed Laser Evaporation (C-MAPLE), to deposit gradient thin films with variable compositions of Sr-substituted hydroxyapatite (SrHA) and ZOL modified hydroxyapatite (ZOLHA) on Titanium substrates. Compositional gradients were obtained by simultaneous laser vaporization of the two distinct material targets. The coatings display good crystallinity and granular morphology, which do not vary with composition. Osteoblast-like MG63 cells and human osteoclasts were co-cultured on the thin films up to 21 days. The results show that Sr counteracts the negative effect of relatively high concentration of ZOL on osteoblast viability, whereas both Sr and ZOL enhance extracellular matrix deposition. In particular, ZOL promotes type I collagen production, whereas Sr increases the production of alkaline phosphatase. Moreover, ZOL exerts a greater effect than Sr on osteoprotegerin/RANKL ratio and, as a consequence, on the reduction of osteoclast proliferation and activity. The deposition method allows to modulate the composition of the thin films and hence the promotion of bone growth and the inhibition of bone resorption.

1. Introduction

Orthopaedic implants require materials with reliable strength, toughness and resistance to wear and corrosion [1,2]. These mechanical requirements are well fulfilled by metallic materials, which however are not able to form a stable bond to bone tissue. Osteointegration can be improved by coating the metal surface with a thin film of calcium phosphate [3]. Functionalization of calcium phosphates with bioactive substances can significantly enhance the performance of the implant. In particular, the positive effect of bisphosphonates (BPs) has been demonstrated on both healthy and osteoporotic animals [4]. As a matter of fact, BPs strongly inhibit bone degradation [5–7], which justifies their widespread employment for the treatment of disorders of bone

* Corresponding author. Fax: +39 051 2099456.
E-mail address: elisa.boanini@unibo.it (E. Boanini).

http://dx.doi.org/10.1016/j.jcis.2015.01.088
0021-9797/

metabolism involving loss of bone substance [8]. Functionalization of calcium phosphate coatings with BPs has been generally achieved by soaking the implant in a BP solution [4]. We have recently shown that it is possible to use Matrix-Assisted Pulsed Laser Evaporation (MAPLE) to synthesize BP-hydroxyapatite (BP-HA), namely alendronate–hydroxyapatite composite coatings [9]. Thanks to the presence of BP, these thin films inhibit osteoclast proliferation and differentiation, whereas they promote osteoblast growth, viability and early differentiation [9]. A similar effect on inhibition of osteoclast activity and promotion of osteoblast differentiation has been reported for strontium via *in vivo* and *in vitro* studies [10,11]. Moreover, the influence of Sr on bone cells is maintained when it is incorporated into HA structure [12–14]. The co-presence of Sr and a potent amino bisphosphonate, zoledronate, in HA nanocrystals has been shown to exhibit a combined, dose dependent, effect on osteoblast promotion and osteoclast inhibition [15].

Recent improvements of MAPLE technique for the biochemical functionalization of surfaces in the field of biomaterials engineering rely upon the development of new concepts for the synthesis of novel materials. The Combinatorial-MAPLE (C-MAPLE) technique is a new approach for the fabrication of gradient organic or inorganic thin films, in view of obtaining bioactive artificial surfaces able to modulate and control cells behavior [16]. Distinct areas of a polymeric binary gradient have been shown to modulate the osteoblast extracellular signal-regulated kinase signaling with different propensity [17]. There are still plenty of challenges to be considered for the third-generation of biomaterials [18]. The goal of this study was the engineering of cell/biomaterial surface interface in order to control cell behavior, with major implications for tissue repair or scaffolds [19].

Due to materials complexity, the conventional "step by step" synthesis of biomaterials with different fixed composition and their subsequent analyses are both time consuming and expensive. With the present study, we propose C-MAPLE as an innovative synthesis method of gradient thin films with variable composition, *in situ* and in a single-step process. The aim is to evaluate the compositional intermixing of Sr-substituted hydroxyapatite (SrHA) and zoledronate modified hydroxyapatite (ZOLHA) for tailoring osteoblast promotion and osteoclast inhibition responses. The fabrication of an array of different chemical and physical features allows cells to be exposed to combinatorial nanostructures to be screened for a synergistic behavior.

2. Materials and methods

2.1. Synthesis and characterization of SrHA and ZOLHA nanocrystals

SrHA nanocrystals were synthesized in N_2 atmosphere using 50 ml of solution with Sr/(Ca + Sr) ratio of 0.1, prepared by dissolving the appropriate amount of $Ca(NO_3)_2{\cdot}4\,H_2O$ and $Sr(NO_3)_2$ in CO_2-free deionized water and adjusting pH to 10 with NH_4OH. The total concentration of $[Ca^{2+}] + [Sr^{2+}]$ was 1.08 M. The solution was heated at 90 °C and 50 ml of 0.65 M $(NH_4)_2HPO_4$ solution, pH 10 adjusted with NH_4OH, was added drop-wise under stirring. The precipitate was maintained in contact with the reaction solution for 5 h at 90 °C under stirring, then centrifuged at 10,000 rpm for 10 min and repeatedly washed with distilled water. The product was dried at 37 °C overnight.

ZOLHA was obtained following the above procedure in the absence of Sr and by adding disodium zoledronate tetrahydrate (Chemos GmbH) to the phosphate solution. Concentration of zoledronate was 14 mM, calculated on final volume.

Powder X-ray diffraction (XRD) patterns were recorded using a PANalytical X'Pert PRO powder diffractometer equipped with a fast X'Celerator detector. Ni-filtered Cu Kα radiation was used (λ = 0.154 nm, 40 mA, 40 kV). For phase identification the 2θ range was investigated from 10 to 60 2θ degrees with a step size of 0.1° and time/step of 100 s. Data used for cell parameters calculations were collected counting for 1200 s at each 0.033° (2θ), and then processed with the Rietveld routine of the HighScore Plus software package (PANalytical).

Calcium and strontium contents in the solid products were monitored by means of an ICP spectrometer (ICP Optima 4200DV, Perkin Elmer). Powders were previously dissolved in 0.1 M HCl. Results from this analysis represent the mean value of three different determinations.

Bisphosphonate content was determined spectrophotometrically via complex formation with Fe(III) ions using a Varian Cary50Bio instrument (λ = 290 nm) [20].

For Transmission Electron Microscopy (TEM) investigations, a small amount of powder was dispersed in ethanol and submitted to ultrasonication. A drop of the suspension was transferred onto holey carbon foils supported on conventional copper microgrids. A Philips CM 100 transmission electron microscope operating at 80 kV was used.

For Fourier Transform-Infrared Spectroscopy (FT-IR) absorption analysis, 1 mg of the powdered sample was carefully mixed with KBr (250 mg, infrared grade) and pelletized under a pressure of 10 tons for 2 min. The pellets were analyzed using a Nicolet 380 FT-IR spectrophotometer to collect 32 scans in the range 4000–400 cm^{-1} with a resolution of 4 cm^{-1}.

2.2. Synthesis and characterization of SrHA and ZOLHA coatings

The experiments of thin coatings deposition were carried out in a vacuum reaction chamber [16,17]. 0.2 g of each powder, SrHA and ZOLHA respectively, were homogenously suspended separately in 20 ml distilled water by ultrasonically stirring. Three ml of each solution were poured into a two concentric ring holder. This way, any possible mixing was avoided. The holder was immersed in liquid nitrogen for 15 min and the solutions were frozen. They were further used as solid targets in the reaction chamber where a cooler supplied with liquid nitrogen flow kept them frozen during multi-pulse laser irradiation and vaporization. We have used a KrF* excimer laser source (λ = 248 nm, τ_{FWHM} = 25 ns) operating at a repetition rate of 3 Hz. The beam was split into two beams, directed by mirrors and focalized with lenses onto the surface of the two concentrically targets, SrHA and ZOLHA respectively (Fig. 1).

In a single experimental run, the synchronized evaporated materials were collected onto 5 distinct Ti substrates of 12 mm diameter. 20,000 laser pulses were applied to grow 0.4 μm thin films, which is sufficient for the *in vitro* tests under considerations. The samples were labelled C-1, C-2, C-3, C-4 and C-5, where the composition varies from C-1 (SrHA) to C-5 (ZOLHA). The set-up allows placing the standard reference compositions (SrHA and

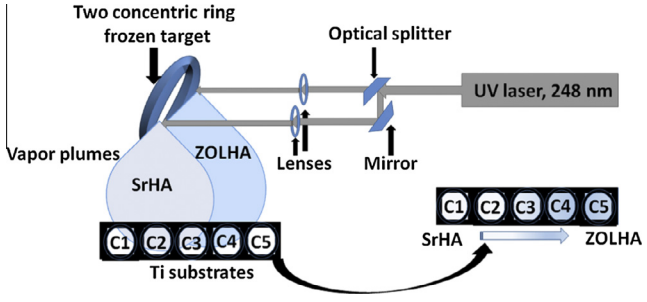

Fig. 1. Schematic of the C-MAPLE set-up.

ZOLHA, respectively) in discrete areas (samples C-1 and C-5) in the same process along with gradient samples (C-2, C-3, C-4) which eliminates false positives or other inaccurate property interpretation of analyses. The experimental conditions for MAPLE transfer and immobilization of SrHA and ZOLHA were carefully adjusted to prevent any thermal damage and irreversible decomposition of materials and are collected in Table 1.

XRD investigations on the coatings were performed using the same powder diffractometer mentioned above. The 2θ range was investigated from 24° to 34° (2θ) with a step size of 0.067° and time/step of 3000 s. The line broadening of the 002 reflection was used to evaluate the length of the coherent domains (τ_{002}) along the *c*-axis. τ_{002} values were calculated from the widths at half maximum intensity ($\beta_{1/2}$) using the Scherrer equation [21]:

$$\tau_{hkl} = (K\lambda)/(\beta_{1/2}\cos\theta)$$

where λ is the wavelength, θ the diffraction angle and K a constant depending on crystal habit (chosen as 0.9). The silicon standard peak 111 was used to evaluate the instrumental broadening.

Morphological investigations of thin films were performed using a Philips XL-20 scanning electron microscope operating at 15 kV. The samples were sputter coated with gold before examination. Energy dispersive X-ray spectrometry (EDS) analyses were carried out on uncoated specimens.

For AFM imaging a Veeco Nanoscope 3D instrument was used. The samples were analyzed in tapping mode using a E scanner (-maximum scan size 15 μm) and phosphorus (n) doped silicon probes (spring constant 20–80 N/m; resonance frequency 250–290 kHz; nominal tip radius < 10 nm). Roughness parameters, namely arithmetic mean roughness (Ra), root-square roughness (Rq), and the vertical distance between the highest and lowest points within the evaluation length (Rt), were recorded.

2.3. In vitro tests

Cell experiments were carried out on coatings deposited on Ti substrates and sterilized by gamma-rays (Cobalt-60) at a dose of 25 kGy. Ti without coating and cells plated on culture plates were tested as reference materials and controls. Human osteoblasts and osteoclasts were co-cultured up to 21 days as described in Supporting Information.

2.3.1. Cell proliferation

Osteoblast and osteoclast proliferation and viability (10 and 21 days) was evaluated by WST1 colorimetric reagent test (WST1, Roche Diagnostics GmbH, Manheim, Germany). The assay is based on the reduction of tetrazolium salt to a soluble formazan salt by a reductase of the mitochondrial respiratory chain, active only in viable cells. 50 μl of WST1 solution and 450 μl of medium (final dilution: 1:10) were added to the osteoblasts and osteoclasts separately, and the multi-well plates were incubated at 37 °C for the next 4 h. Supernatants were quantified spectrophotometrically at 450 nm with a reference wavelength of 625 nm. Results of WST1 are reported as optical density (OD) and directly correlated with the cell number.

2.3.2. Osteoblast activity and differentiation

At the end of experimental times the supernatant was collected from all wells and centrifuged to remove particulates, if any. Aliquots were dispensed in Eppendorf tubes for storage at −70 °C and assayed for Alkaline Phosphatase (ALP, immunoenzymatic assay, USCN Life Science, Wuhan, China), Type I Pro-Collagen (COLL1, immunoassay kit, USCN), Osteoprotegerin (OPG, immunoenzymatic assay, USCN), and Receptor Activator for Nuclear factor KB Ligand (RANKL, immunoenzymatic assay, USCN). Medium additioned with RANKL was evaluated and subtracted from RANKL samples values.

2.3.3. Osteoblast morphology

Samples for each material, at the end of the experiment, were processed for Scanning Electron Microscopy (SEM): osteoblasts grown on the materials were fixed in 2.5% glutaraldehyde, in pH 7.4 phosphate buffer 0.01 M for 1 h and dehydrated in a graded ethanol series. After a passage in hexamethyldisilazane, the samples were air dried. The samples were sputter-coated with Pd prior to examination with a Philips XL20 Scanning Electron Microscope.

2.3.4. Osteoclastogenesis

TRAP-staining was performed to assess osteoclast differentiation according to manufacturer's instructions (SIGMA, Buchs, Switzerland). The positive cells developed red color of different intensity. The number of TRAP-positive multinucleated cells (three or more nuclei each cell) was counted under the microscope and results are given as percentage of CTR.

2.3.5. Statistical analysis

Statistical evaluation of data was performed using the software package SPSS/PC+ Statistics™ 10.1 (SPSS Inc., Chicago, IL USA). The results presented are the mean of six values. Data are reported as

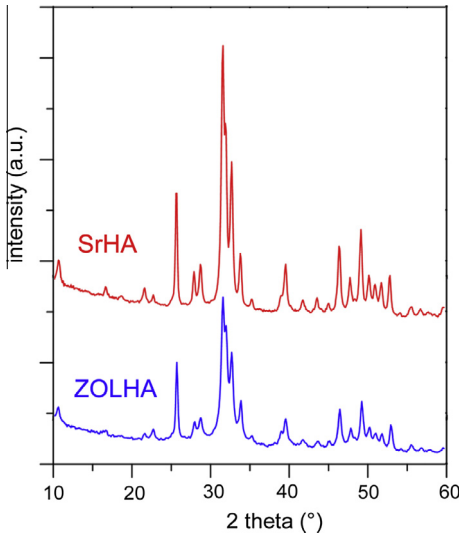

Fig. 2. Powder X-ray diffraction patterns of the as-prepared SrHA and ZOLHA powders.

Table 1
Experimental parameters for C-MAPLE samples synthesis.

Target	Substrate	Substrate temperature	Laser fluence (J cm^{-2})	Dynamic pressure (Pa)	Target-substrate distance (cm)	No. of pulses
ZOLHA (0.2 g in 20 ml H_2O)	5 × Ti	RT	1.6	1	5	20.000
SrHA (0.2 g in 20 ml H_2O)			0.7			

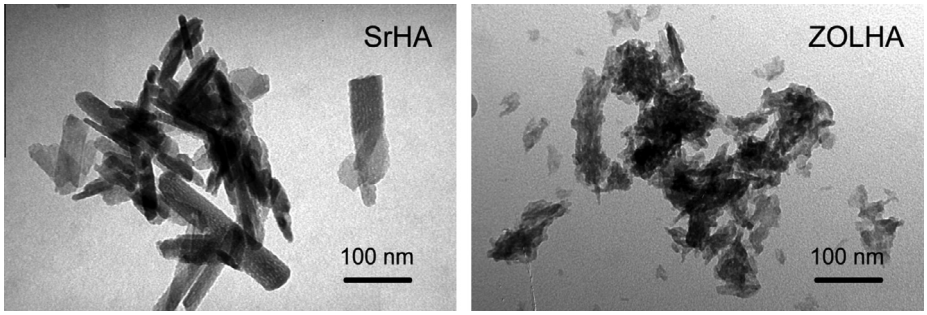

Fig. 3. TEM images of SrHA and ZOLHA nanocrystals.

mean ± standard deviations (SD) at a significance level of $p < 0.05$. After having verified normal distribution and homogeneity of variance, a one-way ANOVA was done for comparison between groups. Finally, a post hoc multiple comparison tests was performed to detect significant differences among experimental groups and control.

3. Results and discussion

3.1. Chemical and structural characterization

The XRD patterns of SrHA and ZOLHA (Fig. 2) indicate that both samples are composed of hydroxyapatite as unique crystalline phase, in agreement with ICDD PDF n.9–432. The XRD pattern of pure HA is reported in Fig. S1 for comparison.

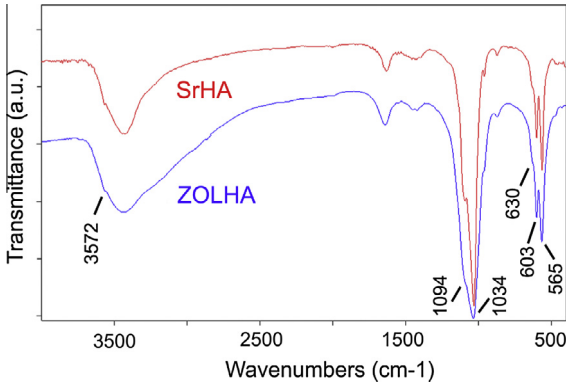

Fig. 4. FT-IR absorption spectra of the as-prepared SrHA and ZOLHA powders.

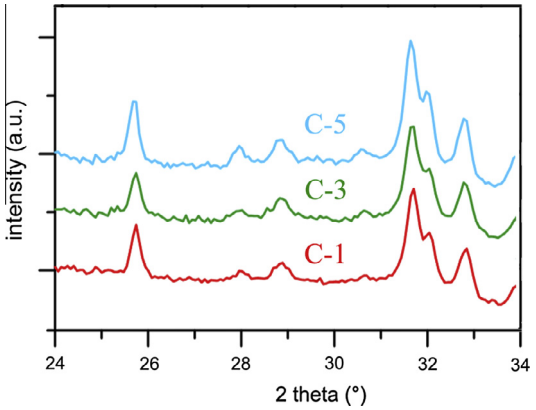

Fig. 5. Powder X-ray diffraction patterns of the C-1, C-3 and C-5 thin films.

Strontium content in SrHA amounts to 8.4 atom%, as revealed by ICP spectrometry. The lattice parameters of SrHA, $a = 9.443(1)$ Å, $c = 6.905(1)$ Å, are enlarged with respect to those characteristic of stoichiometric HA, $a = 9.4269$ Å, $c = 6.8840$ Å [12], coherently with the bigger ionic radius of Sr than Ca. On the other hand, addition of zoledronate does not provoke major variations in the values of the lattice constants, in agreement with previous data [15]. Zoledronate content of ZOLHA, determined through spectrophotometric analysis of the chromophoric complex with FeIII ions [20], is 7.6 wt%. The morphology of HA crystals appears quite affected by the presence of the bisphosphonate: the composite nanocrystals display significantly reduced dimensions, ill defined shapes and edges, with respect to SrHA nanocrystals (Fig. 3), where Sr incorporation induces just minor modifications of the characteristic plate-like morphology of HA nanocrystals (Fig. S1) [13].

The FT-IR absorption spectra of SrHA and ZOLHA powders are reported in Fig. 4a and b, respectively. Both spectra show the characteristic absorption bands of PO_4^{3-} groups in the range 1100–900 cm^{-1} and 610–550 cm^{-1}. Moreover, low intensity absorption bands at 3572 and 630 cm^{-1}, due to OH^-stretching and libration modes, can be appreciated. Weak absorption bands at 1455–1430 cm^{-1} and 870 cm^{-1}. indicate the presence of a very small amount of CO_3^{2-} ions. The FT-IR absorption spectrum of pure HA is reported in Fig. S1 for comparison.

Typical X-ray diffraction patterns of the thin films deposited by C-MAPLE are given in Fig. 5. All the patterns are consistent with the presence of HA as the sole crystalline phase. A qualitative estimation of the size of coherently scattering domains (i.e. the crystallite sizes) along the *c*-axis direction has been calculated from the width at half maximum intensity ($\beta_{1/2}$) of the 002 reflection using the Scherrer equation. The results presented in Table 2 indicate a mean value of the coherent length of the perfect crystalline domains of about 37.4 nm, with no significant variation as a function of composition.

SEM images show that the surface of all thin films is characterized by a granular morphology, with grain dimensions of the order of tens of nanometers, as visible in Fig. 6a and b for sample C-3. Morphology does not exhibit significant variation as a function of composition. A previous study on the interface between the biomimetic apatite layers deposited by MAPLE and Ti substrates

Table 2
Coherent lengths ($_{hkl}$) of the perfect crystalline domains in the direction normal to 002 plane calculated using the Scherrer method, and Sr content (%) evaluated through EDS measurements of the different coatings.

Sample	τ_{002} (nm)	Sr content (atom%)
C-1	38.8 (6)	8.4 (3)
C-2	36.7 (2)	5.8 (3)
C-3	38.1 (11)	4.0 (1)
C-4	37.0 (7)	1.4 (1)
C-5	36.4 (11)	–

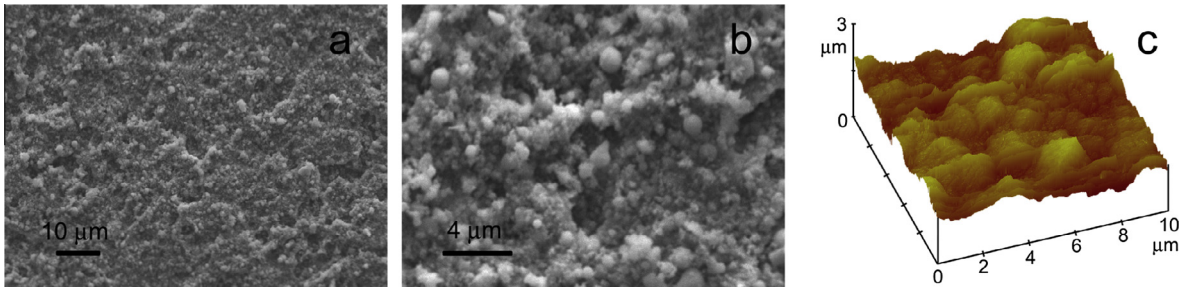

Fig. 6. (a and b) SEM micrographs of C-3 at two different magnifications and (c) AFM image of the surface of C-3.

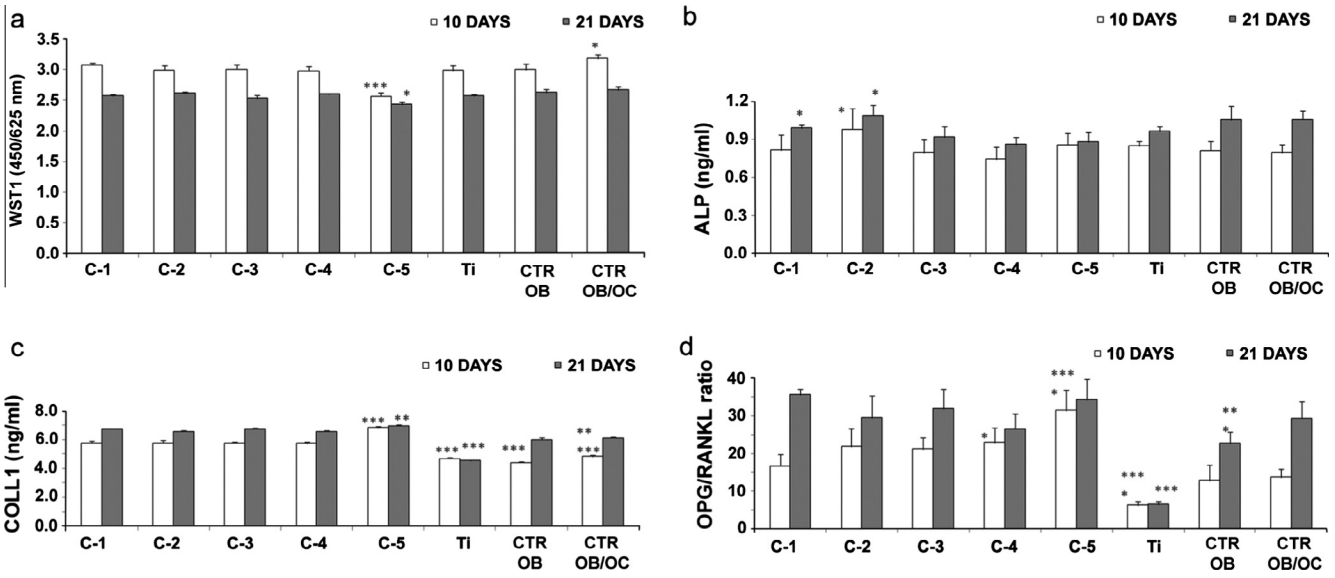

Fig. 7. Osteoblast proliferation (WST1) and activity (ALP, COLL1, OPG/RANKL ratio) in co-cultures with osteoclasts after 10 and 21 days of culture on Ti with different combination of Sr and Zol. (*$p < 0.05$; **$p < 0.005$; ***$p < 0.0001$). a. WST1. 10 days: ***C-5 vs C-1, C-2, C-3, C-4, Ti, CTR OB, CTR OB/OC; *CTR OB/OC vs Ti, CTR OB; 21 days: *C-5 vs CTR OB/OC. b. ALP. 10 days: *C-2 vs C-4; 21 days: *C-1 vs C-4, C-5, *C-2 vs C-3, C-4, C-5. c. COLL1: 10 days: ***C-5 vs C-1, C-2, C-3, C-4, Ti, CTR OB, CTR OB/OC; ***Ti, CTR OB vs C-1, C-2, C-3, C-4; **CTR OB/OC vs C-2; ***CTR OB/OC vs C-1, C-3, C-4; 21 days: *C-5 vs CTR OB/OC; **C-5 vs CTR OB; ***Ti vs C-1, C-2, C-3, C-4, CTR OB, CTR OB/OC. d. OPG/RANKL ratio. 10 days: *C-4 vs CTR OB; ***C-5 vs C-1, CTR OB, CTR OB/OC; *C-5 vs C-2, C-3, C-4; ***Ti vs C-2, C-3, C-4, C-5; *Ti vs C-1; 21 days: ***Ti vs C-1, C-2, C-3, C-4, C-5, CTR OB, CTR OB/OC; **CTR OB vs C-1; *CTR OB vs C-5.

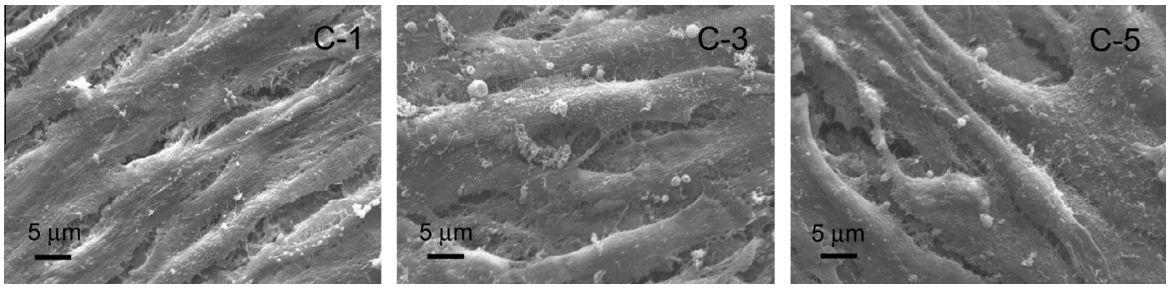

Fig. 8. SEM micrographs of osteoblasts grown on C-1, C-3 and C-5.

[22], evidenced that the films are rather uniform, homogeneous and fairly compact, a clear and net border being visible. Similar organic combinatorial coatings of Levan/Oxidized Levan on glass and silica [17,23], and of fibronectin/Poly-DL-lactide on Si [24] were quite uniform and adherent as visualized in our MAPLE depositions.

In good agreement, the roughness parameters, Ra, Rq and Rt, evaluated by AFM analysis are quite similar for the different samples. Average values were: Ra = 0.291 ± 0.038 µm, Rq = 0.360 ± 0.041 µm, Rt = 2.425 ± 0.093 µm. A typical AFM image is presented in Fig. 6c. It can be concluded that variations in HA composition do not influence coating morphology, as previously found for apatites of different compositions deposited by means of PLD [13,25]. At variance, EDS data clearly pointed to the presence of decreasing amounts of strontium in the coatings on passing from samples C-1 to C-5, that is when changing sample position with respect to the C-MAPLE targets (Table 2). Worth mentioning that Sr content in C-1 sample inferred from EDS measurements is identical with the value measured on target by means of ICP spectrometry.

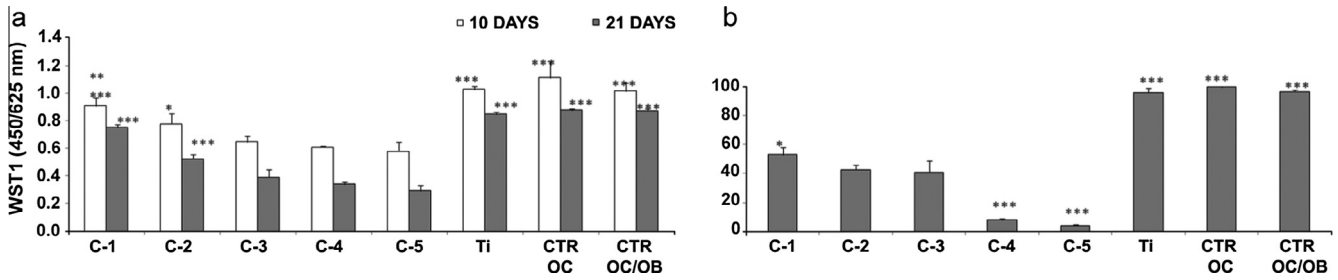

Fig. 9. Osteoclast viability (WST1, 10 and 21 days) and differentiation (TRAP%, 21 days) in co-cultures with osteoblasts on Ti with different combination of Sr and ZOL (**$p < 0.005$; ***$p < 0.0001$). a. WST1. 10 days: **C-1 vs CTR OC; ***C-1 vs C-3, C-4, C-5; *C-2 vs C-4, C-5; ***Ti, CTR OC, CTR OC/OB vs C-2, C-3, C-4, C-5; 21 days: *C-1 vs Ti; ***C-1 vs C-2, C-3, C-4, CTR OC; ***C-2 vs C-3, C-4; ***Ti, CTR OC, CTR OC/OB vs C-2, C-3, C-4, C-5. b. TRAP%. ***Ti, CTR OC, CTR OC/OB vs C-1, C-2, C-3, C-4, C-5; ***C-5, C-4 vs C-1, C-2, C-3; *C-1 vs C-2, C-3.

Elemental mapping indicates that Sr and Ca distribution is homogeneous within the coatings, as shown in Fig. S2 for C-3 sample.

3.2. Osteoblast and osteoclast co-culture activity

Osteoblast and osteoclast were co-cultured on SrHA and ZOLHA deposited in different relative amounts on Ti disks using combinatorial-MAPLE, i.e. C-1 to C-5 samples. The use of co-culture permits to evaluate the interaction among cells, materials and drugs and it simulates the *in vivo* microenvironment where cells influence each other during the processes of bone remodeling. Osteoblast proliferation and viability was evaluated after 10 and 21 days of co-culture in experimental samples and controls (Fig. 7a). At 10 days CTR OB/OC shows a significant enhancement of cell proliferation in comparison to CTR OB and Ti. On the contrary, C-5 (ZOLHA) group at 10 days shows a significant reduction of osteoblast viability when compared to experimental groups and controls, while at 21 days the difference is maintained only with respect to CTR OB/OC.

The results of the evaluation of the most common markers of osteoblast differentiation are reported in Fig. 7b and c. The activity of ALP is significantly higher on C-1 (SrHA) group than on C-4 and C-5 (21 days), and on C-2 group when compared to C-4 (10 and 21 days), C-3, and C-5 (21 days). The production of COLL1 appears enhanced on C-5 group in comparison with all other groups (10 days) and CTRs (10 and 21 days). Ti (10 and 21 days), CTR OB and CTR OB/OC (21 days) are significantly lower than experimental groups. SEM images show that at the end of the experimental times all the samples are covered with well attached and spread osteoblasts. The cells appear rich of filopodia, as shown in Fig. 8 for sample C-1, C-3 and C-5.

Both Sr and ZOL have been reported to inhibit osteoclastogenesis and to influence osteoblast proliferation, viability and differentiation [14,26–29]. While the anti-osteoclastogenesis activity of ZOL is well established, its effects on osteoblasts are strictly dose dependent. In particular, a cytotoxic effect of high concentrations of amino-bisphosphonates has been reported [30]. The results of the present study on osteoblast response are consistent with those previously reported [15,27,30–33] and confirm a reduction of cell viability at relatively high concentration of ZOL, as in C-5 group. On the other hand, Sr incorporation into HA coating does not display any negative effect on osteoblast response. At lower concentration and in combination with different amount of Sr, ZOL does not exhibit significant cytotoxicity whereas it shows a positive effect on extracellular matrix deposition. In fact, ZOL promotes COLL1 production, whereas Sr significantly increases the production of ALP.

The induction of osteoclast differentiation depends on microenvironment and on osteoblast signaling products, moreover Sr and ZOL are known to modulate OPG expression by osteoblasts, modifying OPG/RANKL ratio [34]. On this basis, we investigated OPG and RANKL production on the different samples. In fact these molecules, expressed by osteoblasts following various stimulations, are known to be essential for regulating osteoclast differentiation [35]. As reported in Fig. 7d, OPG/RANKL ratio shows the lowest value on Ti group when compared to all other groups (10 and 21 days) and CTRs (21 days). On the contrary at 10 days C-5 is significantly higher than C-1, C-2, C-3, C-4 and CTRs. CTR OB is also lower than C-4 (10 days), C-1 and C-5 (21 days). Previous studies [31,36,37] suggest that the interplay biomaterial/osteoblast/osteoclast affects more significantly the production of OPG with respect to RANKL. Results of OPG/RANKL ratio in the present study are mainly due to the significant production of OPG by cells grown on experimental coatings in comparison to Ti, CTR OB and CTR OB/OC, whereas RANKL level is not particularly affected by coating composition (data not shown). In agreement with the results of OPG/RANKL ratio, osteoclast proliferation on all experimental groups is significantly lower than on Ti and CTR groups, at 10 and 21 days (Fig. 9a). OPG blocks the RANKL-RANK link and it counteracts bone-resorbing activity, as it is associated to a decrease of osteoclast number. In agreement, the results show that osteoclast viability and activity is deeply influenced by the presence of both Sr and ZOL, in a dose dependent way. In particular, C-1 group displays a significantly higher WST-1 value than C-3, C-4 (10 and 21 days), C-5 (10 days) and C-2 (21 days). Moreover, C-2 group displays a higher viability when compared to C-4 (10 and 21 days), C-5 (10 days) and C-3 (21 days).

The evaluation of TRAP (Fig. 9b) shows a regular osteoclastogenesis on Ti and CTR groups, while experimental groups demonstrate the effect of Sr and ZOL on osteoclast differentiation and activity, also in correlation with WST1 and OPG/RANKL ratio results (Pearson correlation test, $p < 0.001$). In particular, TRAP% of C-5 and C-4 is significantly reduced when compared to C-1, C-2, and C-3. Moreover C-1 is higher than C-2 and C-3.

Bone formation and resorption depends on osteoblast and osteoclast, whose activity is interlinked. For this reason, the choice of co-cultured cells is crucial for understanding cell behavior when cultured in presence of drug and biomaterials. Overall data indicate the positive and the negative aspects of Sr and ZOL treatment when they are used alone: Sr enhances osteoblast viability and activity in comparison with ZOL, but it is less efficient than ZOL in affecting osteoclastogenesis. Their association allows to overcome their singular negative effects and to modulate their combined action.

4. Conclusions

Crystalline thin films with a gradient composition of Sr-substituted hydroxyapatite and zoledronate containing hydroxyapatite have been successfully deposited on Titanium substrates by the

innovative Combinatorial-MAPLE technique. Osteoblast and osteoclast behavior when co-cultured on the coatings depends on the relative content of Sr and ZOL. The inhibitory action of ZOL on osteoclast viability and activity is more efficient than that of Sr, which plays a greater beneficial role on osteoblast proliferation and viability. The data demonstrate that it is possible to apply C-MAPLE to synthesize coatings with tailored composition, which provides modulated local availability of Sr and ZOL and, as a consequence, promotion of bone growth and prevention of bone resorption according to specific requirements.

Acknowledgments

This research was carried out with the financial support of University of Bologna (FARB 2012), MIUR (FIRB n°RBAP10MLK7) and contract 19-RO-FR.

Appendix A. Supplementary material

Supplementary data associated with this article can be found, in the online version, at http://dx.doi.org/10.1016/j.jcis.2015.01.088.

References

[1] K. Duan, R. Wang, J. Mater. Chem. 16 (2006) 2309–2321.
[2] T.J. Webster, Nanophase ceramics: the future orthopedic and dental implant material, in: J.Y. Ying (Ed.), Nanostructured Materials, Academic Press, New York, 2001, pp. 125–166.
[3] R.A. Surmenev, M.A. Surmeneva, A.A. Ivanova, Acta Biomater. 10 (2014) 557–559.
[4] S. Niu, X. Cao, Y. Zhang, Q. Zhu, J. Zhu, J. Surg. Res. 179 (2013) 107–115.
[5] H. Fleisch, R.G. Russell, M.D. Francis, Science 165 (1969) 1262–1264.
[6] R.G. Russell, N.B. Watts, F.H. Ebetino, M.J. Rogers, Osteoporos Int. 19 (2008) 733–759.
[7] E.V. Giger, B. Castagner, J.C. Leroux, J. Control Release 167 (2013) 175–188.
[8] R.G.G. Russell, Bone 49 (2011) 2–19.
[9] A. Bigi, E. Boanini, C. Capuccini, M. Fini, I.N. Mihailescu, C. Ristoscu, F. Sima, P. Torricelli, Biomaterials 30 (2009) 6168–6177.
[10] P.J. Marie, Osteoporos Int. 16 (2005) S7–S10.
[11] E. Bonnelye, A. Chabadel, F. Saltel, P. Jurdic, Bone 42 (2008) 129–138.
[12] C. Capuccini, P. Torricelli, E. Boanini, M. Gazzano, R. Giardino, A. Bigi, J. Biomed. Mater. Res. A 89A (2009) 594–600.
[13] C. Capuccini, P. Torricelli, F. Sima, E. Boanini, C. Ristoscu, B. Bracci, G. Socol, M. Fini, I.N. Mihailescu, A. Bigi, Acta Biomater. 4 (2008) 1885–1893.
[14] E. Boanini, P. Torricelli, M. Fini, A. Bigi, J. Mater. Sci. Mater. Med. 22 (2011) 2079–2088.
[15] E. Boanini, P. Torricelli, M. Gazzano, E. Della Bella, M. Fini, A. Bigi, Biomaterials 35 (2014) 5619–5626.
[16] F. Sima, E. Axente, L.E. Sima, U. Tuyel, M.S. Eroglu, N. Serban, C. Ristoscu, S.M. Petrescu, E.T. Oner, I.N. Mihailescu, Appl. Phys. Lett. 101 (2012) 233705.
[17] E. Axente, F. Sima, L.E. Sima, M. Erginer, M.S. Eroglu, N. Serban, C. Ristoscu, S.M. Petrescu, E.T. Oner, I.N. Mihailescu, Biofabrication 6 (2014) 035010.
[18] L.L. Hench, J.M. Polak, Science 295 (2002) 1014–1017.
[19] M.M. Stevens, J.H. George, Science 310 (2005) 1135–1138.
[20] J. Kuljanin, I. Janković, J. Nedeljković, D. Prstojević, V. Marinković, J. Pharm. Biomed. Anal. 28 (2002) 1215–1220.
[21] H.P. Klug, L.E. Alexander, X-ray Diffraction Procedures for Polycrystalline and Amorphous Materials, Wiley-Interscience, New York, 1974.
[22] A. Visan, D. Grossin, N. Stefan, L. Duta, F.M. Miroiu, G.E. Stan, M. Sopronyi, C. Luculescu, M. Freche, O. Marsan, C. Charvillat, S. Ciuca, I.N. Mihailescu, Mater. Sci. Eng. B (2014) 56–63.
[23] F. Sima, E. Cansever Mutlu, S.E. Mehmet, L. Sima, N. Serban, C. Ristoscu, S. Petrescu, E. Toksoy Oner, I.N. Mihailescu, Biomacromolecules 12 (6) (2011) 2251–2256.
[24] F. Sima, E. Axente, I. Iordache, C. Luculescu, O. Gallet, K. Anselme, I.N. Mihailescu, Appl. Surface Sci. 306 (2014) 75–79.
[25] E. Gyorgy, P. Torricelli, G. Socol, M. Iliescu, I. Mayer, I.N. Mihailescu, A. Bigi, J. Werckman, J. Biomed. Mater. Res. A 71 (2004) 353–358.
[26] K.L. Wong, C.T. Wong, W.C. Liu, H.B. Pan, M.K. Fong, W.M. Lam, W.L. Cheung, W.M. Tang, K.Y. Chiu, K.D.K. Luk, W.W. Lu, Biomaterials 30 (2009) 3810–3817.
[27] E. Boanini, P. Torricelli, M. Gazzano, M. Fini, A. Bigi, Biomaterials 33 (2012) 722–730.
[28] B. Pan, A.N. Farrugia, L.B. To, D.M. Findlay, J. Green, K. Lynch, A.C. Zannettino, J. Bone Miner. Res. 19 (2004) 147–154.
[29] S.J. Suratwala, S.K. Cho, J.J. van Raalte, S.H. Park, S.W. Seo, S.S. Chang, T.R. Gardner, F.Y.I. Lee, J. Bone Joint Surg. Am. 90 (2008) 2189–2196.
[30] I.R. Orris, J. Cell Biochem. 106 (2009) 109–118.
[31] S. Grainer, A. Kadow-Romacker, G. Schmidmaier, B. Wildemann, J. Biomed. Mater. Res. 91A (2009) 288–295.
[32] A. Naidu, P.C. Dechow, R. Spears, J.M. Wright, H.P. Kessler, L.A. Opperman, Oral. Surg. Oral. Med. Oral. Pathol. Oral. Radiol. Endod. 106 (2008) 5–13.
[33] J. Wang, L. Zhang, X. Sun, X. Chen, K. Xie, M. Lin, G. Yang, S. Xu, W. Xia, Z. Gou, Biomed. Mater. 9 (4) (2014) 045002.
[34] S. Peng, X.S. Liu, S. Huang, Z. Li, H. Pan, W. Zhen, K.D.K. Luk, X.E. Guo, W.W. Lu, Bone 49 (2011) 1290–1298.
[35] T. Takagiri, N. Takahashi, Oral Diseases 8 (2002) 147–159.
[36] G.J. Atkins, K.J. Welldon, P. Halbout, D.M. Findlay, Osteoporos Int. 20 (2009) 653–664.
[37] H.C. Schroder, X.H. Wang, M. Wiens, B. Diehl-Seifert, K. Kropf, U. Schlossmacher, W.E.G. Muller, J. Cell Biochem. 113 (2012) 3197–3206.